



**VHF AND MICROWAVE RADIATION EMITTED BY
LIGHTNING AND ITS EFFECT TOWARDS 4G LTE
WIRELESS COMMUNICATION**



SHAMSUL AMMAR BIN SHAMSUL BAHARIN

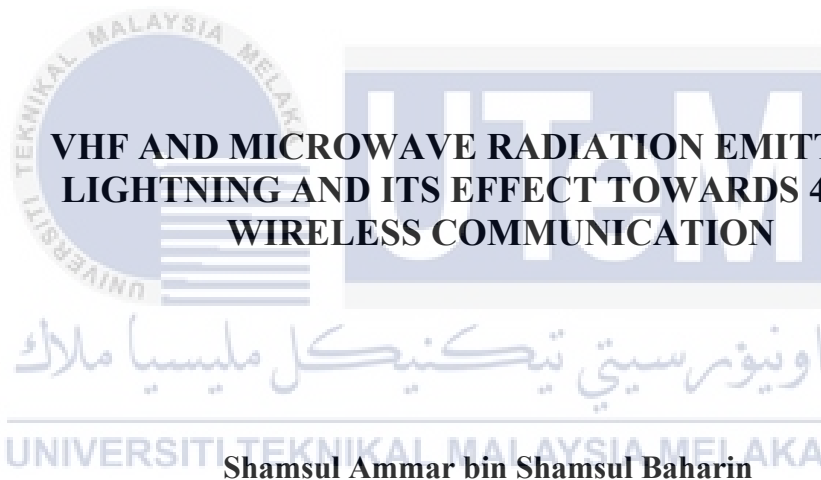
UNIVERSITI TEKNIKAL MALAYSIA MELAKA

DOCTOR OF PHILOSOPHY

2024



**Faculty of Electronics and Computer Technology and
Engineering**



Doctor of Philosophy

2024

**VHF AND MICROWAVE RADIATION EMITTED BY LIGHTNING AND ITS
EFFECT TOWARDS 4G LTE WIRELESS COMMUNICATION**

SHAMSUL AMMAR BIN SHAMSUL BAHARIN



UNIVERSITI TEKNIKAL MALAYSIA MELAKA

2024

DEDICATION

Gratitude towards the past of myself for all the time and effort had been spent;

Thanks for the supports from my parents;

Thanks, ALLAH SWT, for granting me the opportunity to collect data from the
thunderstorms;

Along the journey of completing this thesis.



ABSTRACT

Electric breakdown process starts with electron avalanche, and then streamer and lastly become leader. They initiate almost all types of lightning flashes except narrow bipolar event (NBE) that was believed to be initiated by fast breakdown. This thesis explores the temporal characteristics of microwave and very high frequency (VHF) electric field radiations associated with the conventional breakdown of stepped leader pulses (SLPs) from negative cloud-to-ground (-CG) flash and fast breakdown of NBEs. The primary motivation is to discern whether both microwave and VHF radiations emitted from the same process or originated from different sources. In existing literature, propagating streamers are identified as the source of VHF radiation emission, while microwave radiation from lightning resulted from head-on collisions of streamers and electron avalanche/corona breakdown at the tip of the leader. Considering that The Fourth Generation Long Term Evolution (4G LTE) mobile links operate in the microwave band, potential interference effects during data transmission need to be investigated as lightning also radiated well at microwave band. To address these objectives, three different measurement setups were designed. First, an experimental setup consisted of fast and slow-varying antennas and radio sensors to capture the temporal characteristics of microwave and VHF radiation associated with SLPs and NBEs. Additionally, a VHF interferometer was implemented to observe the direction and propagation of velocities as well as the altitude height of the VHF radiation sources of NBEs. Furthermore, the study integrated measurements of lightning electric field and 4G LTE performance to assess potential interference effects during data transmission. The noteworthy findings of this study reveal that the sources of microwave and VHF radiation associated with both electrical breakdowns originate from different sources, as evidenced by the temporal analysis of the onset time differences. Further analysis indicates that positive NBEs exhibited a 46% bigger for onset time difference between microwave radiation and VHF emissions, compared to SLPs. In contrast, negative NBEs demonstrated an even more remarkable 85% bigger in the same context. Moreover, when examining the VHF radiation associated with positive and negative NBEs in relation to the onset of fast electric field, positive NBEs displayed a 62% bigger compared to SLPs while negative NBEs exhibited an astonishing 88% bigger. These results suggest that the speed of electron avalanches and streamers of fast breakdown of NBEs is faster compared to the conventional electron avalanches and streamers of SLPs. Additionally, the VHF interferometer mapping reveals that the VHF radiation sources for NBEs propagate bidirectionally with a propagation speed reaching 10^8 ms^{-1} . After comparing the performance of 4G LTE data transmission in both fair weather and thunderstorms, minimal impact was observed during fair weather. However, disruptions were reported during three reported thunderstorms, affecting either the client or server nodes. Furthermore, -CG and intra-cloud (IC) flashes were identified as the main factors that interrupted the data transmission.

SINARAN VHF DAN GELOMBANG MIKRO YANG DIPANCARKAN KILAT DAN KESANNYA TERHADAP KOMUNIKASI WAYARLES 4G LTE

ABSTRAK

Proses pemecahan elektrik bermula dengan longSORan elektron, kemudian penjurus dan terakhir pemimpin. Mereka memulakan hampir semua jenis kilat kecuali peristiwa bipolar sempit (NBE) yang dipercayai dimulakan oleh pemecahan pantas. Tesis ini meneroka ciri-ciri temporal gelombang mikro dan sinaran medan elektrik frekuensi sangat tinggi (VHF) yang dikaitkan dengan pemecahan konvensional pemimpin berperingkat (SLP) daripada kilat awan-ke-tanah negatif (-CG) dan pemecahan pantas NBE. Motivasi utama adalah untuk membezakan sama ada sinaran gelombang mikro dan VHF berpunca daripada proses yang sama atau berasal dari sumber yang berbeza. Dalam kesusasteraan sedia ada, pergerakan penjurus dikenal pasti sebagai sumber pancaran sinaran VHF, manakala sinaran gelombang mikro daripada kilat berasal daripada perlanggaran depan kepala penjurus dan pemecahan elektron/korona di hujung pemimpin. Memandangkan pautan mudah alih Generasi Keempat Evolusi Jangka Panjang (4G LTE) beroperasi dalam jalur gelombang mikro yang dipancarkan sangat baik oleh kilat, potensi kesan gangguan semasa penghantaran data perlu disiasat. Pertama, persediaan eksperimen terdiri daripada antena medan elektrik cepat dan lambat berubah-ubah dan penerima radio untuk menangkap ciri temporal gelombang mikro dan sinaran VHF yang dikaitkan dengan SLP dan NBE. Selain itu, interferometer VHF telah dilaksanakan untuk memerhatikan arah dan perambatan halaju serta ketinggian sumber sinaran VHF bagi kedua-dua jenis NBE. Tambahan pula, kajian ini menggabungkan pengukuran medan elektrik kilat dan prestasi 4G LTE untuk menilai potensi kesan gangguan medan elektromagnetik semasa penghantaran data. Penemuan penting kajian ini mendedahkan bahawa sumber gelombang mikro dan sinaran VHF yang dikaitkan dengan kedua-dua pemecahan elektrik berasal daripada sumber yang berbeza, seperti yang dibuktikan oleh analisis temporal bagi perbezaan masa permulaan. Analisis lebih lanjut menunjukkan bahawa NBE positif menunjukkan 46% lebih besar perbezaan masa permulaan antara radiasi gelombang mikro dan pelepasan VHF berbanding dengan SLPs. Sebaliknya, NBE negatif menunjukkan 85% lebih besar dalam konteks yang sama. Di samping itu, apabila mengkaji radiasi VHF yang dikaitkan dengan positif dan negatif NBE berkaitan dengan permulaan medan elektrik yang cepat, positif NBE menunjukkan 62% lebih besar berbanding SLPs manakala negatif NBEs menunjukkan peningkatan 88% yang menakjubkan. Keputusan ini menunjukkan bahawa kelajuan longSORan elektron dan penjurus bagi kedua-dua jenis NBE adalah lebih pantas berbanding dengan kelajuan longSORan elektron konvensional dan penjurus SLP. Selain itu, pemetaan interferometer VHF mendedahkan bahawa sumber gelombang VHF untuk NBE positif dan negatif bergerak secara dua arah dengan kelajuan mencapai 10^8 ms^{-1} . Selepas membandingkan prestasi penghantaran data 4G LTE dalam cuaca cerah dan ribut petir, kesan minimum diperhatikan semasa cuaca cerah. Walau bagaimanapun, gangguan telah dilaporkan semasa tiga ribut petir yang menjejaskan sama ada nod pelanggan atau pelayan. Tambahan pula, -CG dan awan intra (IC) dikenal pasti sebagai faktor utama yang mengganggu penghantaran data.

ACKNOWLEDGEMENTS

All praises to Allah, the Lord of the universe. Blessings and greetings to Prophet Muhammad SAW, his entire family, his companions, and the descendants of his descendants.

First and foremost, I would like to express my sincere gratitude to my supervisor, Associate Professor Dr. Mohd Riduan Bin Ahmad, and my co-supervisor, Associate Professor Dr. Mohamad Zoinol Abidin Bin Abd. Aziz, from the Faculty of Electronics Engineering and Computer Engineering (FTKEK), Universiti Teknikal Malaysia Melaka (UTeM), Durian Tunggal, Melaka, Malaysia, for their unwavering support, guidance throughout the projects, and encouragement in completing this thesis.

I extend heartfelt thanks to my parents, Shamsul Baharin and Hanaiti, for the continuous support they have provided throughout the completion of this thesis. Additionally, I am grateful to my brother, Arifie, along with his wife, Sabaria, and my sister, Umi and her husband, Hafiz, for their steadfast support until the successful completion of my study. Special appreciation goes to my beloved nieces, Aisyah and Aminah, whose cuteness never failed to bring a smile to my face.

I would like to express a million thanks and applause to Dr. Haziq, Sulaiman, Seah, Ammar Jr., Antony, Afiq, Haikal, Rifhan, Suci, Zuhair, Uwais, Amal, Aizat, Muz, Zahin, and Aniq for their companionship, support, and invaluable assistance during my research studies. I look forward to the possibility of reuniting and meeting again on future occasions.

UNIVERSITI TEKNIKAL MALAYSIA MELAKA

TABLE OF CONTENTS

	PAGE
DECLARATION	
APPROVAL	
DEDICATION	
ABSTRACT	i
ABSTRAK	ii
ACKNOWLEDGEMENTS	iii
TABLE OF CONTENTS	iv
LIST OF TABLES	vii
LIST OF FIGURES	viii
LIST OF ABBREVIATIONS	xiv
LIST OF PUBLICATIONS	xvii
CHAPTER	
1. INTRODUCTION	1
1.1 Introduction	1
1.2 Research background	1
1.3 Problem statement	3
1.4 Objectives	5
1.5 Scopes of research	6
1.6 Contribution of research work	8
1.7 Thesis organization	9
2. LITERATURE REVIEW	11
2.1 Introduction	11
2.2 Charge structure inside the cloud	11
2.3 Electrical breakdown process	13
2.3.1 Conventional breakdown	14
2.3.2 Fast breakdown	21
2.4 Electromagnetic radiation emitted by lightning	26
2.5 Low frequency radiation component	27
2.5.1 Fast and slow-varying electric field	27
2.5.2 Cloud-to-ground lightning flashes	29
2.5.3 Cloud lightning flashes	32
2.6 High frequency radiation	33
2.6.1 Microwave radiation emitted by lightning flashes	33
2.6.2 Fourier transform	34
2.6.3 Direct measurement	37
2.6.4 Simulation studies	49
2.7 Wi-fi vs 4G LTE	53
2.8 Lightning interference effects on communication links	55
2.9 Critical review	59
2.10 Summary	62

3.	METHODOLOGY	63
3.1	Introduction	63
3.2	General flow of research	63
3.3	Experimental setup and instrumentation	65
3.3.1	Antenna design to measure low and high frequency electric fields	66
3.3.2	Fast and slow electric field buffer circuits	77
3.3.3	Radio systems to measure microwave and VHF radiation	85
3.3.4	Digitizers	87
3.3.5	Design and development of lightning measurement systems	88
3.4	Validation of thunderstorms	90
3.4.1	Electric field mill	91
3.4.2	Observation from CAPPI radar	92
3.4.3	Magnetic direction finder	93
3.4.4	Lightning Detection System (LDS)	95
3.4.5	VHF interferometer and angular uncertainties	97
3.5	Parameters measured at low and high frequency electric fields	103
3.6	4G LTE network performance measurement	106
3.7	Summary	110
4.	EVALUATION OF VHF MICROWAVE RADIATION EMITTED BY CONVENTIONAL AND FAST BREAKDOWN EVENTS	111
4.1	Introduction	111
4.2	Stepped leader of -CG flash	111
4.2.1	Locations of -CG flashes	112
4.2.2	Temporal characteristics	116
4.2.3	Microwave radiation associated with stepped leader pulses	117
4.2.4	Characterization of quiet period	119
4.2.5	Microwave radiation associated with quiet period	121
4.2.6	Onset time difference	123
4.3	Negative NBE	125
4.3.1	Details and locations of -NBE	125
4.3.2	Electric field and VHF radiation associated with -NBE	128
4.3.3	The VHF interferometer mapping of -NBE	130
4.3.4	Microwave radiation associated with -NBE	134
4.4	Positive NBE	136
4.4.1	Details and locations of +NBE	136
4.4.2	Microwave and VHF radiation associated with +NBE	139
4.4.3	The VHF interferometer mapping for isolated +NBE	141
4.4.4	The VHF interferometer mapping for +NBE that initiated IC and -CG	143
4.5	Discussion	148
4.5.1	Sources of microwave and VHF radiation emitted from lightning flashes	148
4.5.2	Conventional breakdown of stepped leader	149
4.5.3	Fast breakdown of NBE	153
4.5.4	Propagation of VHF radiation sources during fast breakdown	155
4.6	Summary	158

5. CORRELATION ANALYSIS OF LIGHTNING INTERFERENCE TOWARDS 4G LTE MOBILE COMMUNICATION	159
5.1 Introduction	159
5.2 4G LTE performance analysis	159
5.2.1 Fair-weather conditions	160
5.2.2 Network performance analysis of Storm 1 and 2	163
5.2.3 Network performance analysis of Storm 3 and 4	167
5.3 Discussion	170
5.3.1 Part 1	170
5.3.2 Part 2	172
6. CONCLUSIONS AND FUTURE WORKS	177
6.1 Conclusion	177
6.2 Future works and recommendation	179
REFERENCES	181
APPENDIX A	191



LIST OF TABLES

TABLE	TITLE	PAGE
2.1	Temporal characteristics of the lightning processes in CG flash (Cooray, 2015).	30
2.2	Summary on microwave radiations detected by direct measurements.	47
2.3	Wi-fi standards based on Institute of Electrical and Electronics Engineers (IEEE).	54
2.4	Difference between conventional breakdown and fast breakdown.	61
3.1	Specification of the three main lightning detection system used in this thesis.	65
3.2	Values of the areas and capacitance of the fast antenna (A3) and VHF antenna (A4).	67
3.3	Value of impedance of FR4 with its copper patch of A3 and A4 size.	67
3.4	Parameter lists of the finite antenna.	73
3.5	List of components for both buffer circuits.	80
3.6	Specifications of the three PicoScope series.	88
3.7	Conditions for positive polarity lightning flashes.	94
3.8	Conditions for negative polarity lightning flashes.	95
4.1	Details of the ten lightning flashes (-CG) within reversal distance chosen for analysis.	113
4.2	Details of the -NBEs.	126
4.3	Amplitudes of the multiple peaks of the -NBEs.	130
4.4	Details of -NBEs associated with microwave radiations.	135
4.5	Details of the +NBEs.	138
4.6	Summary collected data of positive and negative NBEs	153
5.1	The details of fair-weather and storms selected for the analysis.	160
5.2	The 4G LTE network performance during fair-weather.	162

LIST OF FIGURES

FIGURE	TITLE	PAGE
2.1	Tripole charge structure that typical for a thundercloud to exist before lightning happens (Figure created by author).	13
2.2	Townsend electron avalanche visualisation. Note that the liberated electron (magenta dot) will continue colliding with another air molecule to liberate another new electron (new magenta dot) while the former electron is now indicated by the black dot.	17
2.3	Example of mechanism (a) positive streamer and (b) negative streamer (c) midgap streamer (Cooray, 2015).	20
2.4	Example of mechanism (a) positive leader and (b) negative leader (Cooray, 2015).	21
2.5	The visual diagram for FPB and FNB associated with +NBE and -NBE (Figure created by author).	23
2.6	Mixed fast breakdown as proposed by Huang et al. (2021).	25
2.7	The rebounding MTLE model of streamer-based NBEs, (I)–(III) are different growth stages of the streamer corona system of NBEs (Li et al., 2022).	26
2.8	Diagram of charge displaced from the sphere and direction of electric field (Cooray, 2015).	29
2.9	Example of a –CG flash captured from Malaysia thunderstorm on 29 November 2012 reported Ahmad et al. (2014) that shows multiple stokes.	31
2.10	Example of +CG flash with 4 return (Baharudin et al., 2016).	32
2.11	Examples of -NBE (left) and +NBE (right) recorded by Ahmad et al. (2010).	33
2.12	(a) Electric field waveform for the first return stroke (b) Fourier transform of the first return stroke obtained during Thunderstorm Research International Project (TRIP; Pierce, 1976).	36
2.13	The plot of normalized spectrum at 50 km of first return stroke.	36
2.14	Waveforms of intracloud events (left) and their respective frequency domain on the right as reported by Weidman et al. (1981). Furthermore, solid lines on the right were frequency domain of return stroke from Figure 2.12 plotted as reference.	37

2.15	The frequency domain data from lightning that was acquired using radio frequency (filter-detector) techniques.	39
2.16	Schematic diagram for the setup of measurement by Brook and Kitagawa (1964).	39
2.17	Schematic of measurement setup by Kosarev research group (Kosarev et al., 1970).	41
2.18	Schematic diagram of the measurement setup by Rust et al. (1979).	42
2.19	Schematic diagram of the measurement setup by Le Boulch et al. (1987).	43
2.20	Block diagram of the radiometer used by Fedorov et al. (2001). Note that (f) represents fine channel while (c) represents coarse channel; e.g. PD(f) and PD(c) are the peak detectors of the fine and coarse channels.	43
2.21	Diagram of measuring site by Satoru Yoshida.	44
2.22	Diagram for setup of lightning remote sensing system (Ahmad et al., 2013).	45
2.23	Schematic diagram for apparatus setup by Peterson and Beasley (2013).	46
2.24	Visual diagram of Seah (2020) deployed in Malacca.	47
2.25	Frequency spectrum of critical avalanches growing at the tip of streamer in 3 field configurations; pointed (a), co-axial (b), spherical (c).	50
2.26	Simulations of streamer propagating from opposite directions separated by 30 cm gap (Luque, 2017).	52
2.27	Simulation results of two bidirectional propagating streamers (Shi, 2019).	53
2.28	Overall figure of the experimental setup by Esa et al. (2005).	56
2.29	Wireless router, server and client configurations used in Ahmad et. al (2012).	57
2.30	Experimental setup recording BER and CLD by Ahmad et. al (2014).	58
3.1	General flow of the research work.	64
3.2	Response impedance. The blue plot is for the A3 size parallel plate antenna and the red plot is for the A4 size parallel plate antenna.	68
3.3	Flow-chart on completing a parallel plate antenna.	69
3.4	Example of parallel plate antenna with distance of 3 cm air gap using CST software simulation.	70
3.5	Example of the electric field flows in three-dimension (3D) forms.	70
3.6	An example of the direction of the electric field is downwards vertically.	70
3.7	A3 size parallel plate antenna with 3 cm gap between the plates to measure electric field below than 3 MHz.	71
3.8	FR4 A4 size parallel plate antenna with 1 cm gap between the plates to measure VHF electric field signal at 60 MHz. (a): side view; (b) top view; (c) bottom view.	71
3.9	Antenna design structure of finite antenna in CST. (a): Structure of top plate. (b): Structure of ground plate. (c): Separation between two plates (air gap). (d) overview of the finite antenna designed. (Note that yellow region is copper patch while white region is FR-4 substrate).	73

3.10	Return loss ($S_{1,1}$) simulation results of the finite antenna across different height of air gap. (a): 10 mm to 40 mm air gap; (b): 5 mm to 20 mm air gap; (c): 11 mm to 20 mm air gap; (d): the $S_{1,1}$ when d equal to 16 mm.	74
3.11	Simulation results of radiation pattern of the finite antenna at 0.97 GHz. (a) shows the 3D view while (b) presents the polar plot of the radiation pattern obtained.	75
3.12	The calibration of the finite antenna under far-field measurement in Anechoic chamber.	76
3.13	Return loss of the finite antenna measured by VNA.	76
3.14	Radiation patterns of finite antenna in far field measurement at 0.97 GHz.	77
3.15	Overall process flow of constructing electric field sensor for lightning remote sensing system.	78
3.16	Designing buffer circuit for fast electric field using Multisim software.	80
3.17	Flow of the fabrication process PCB board.	81
3.18	Ultraviolet (UV) Expose machine.	82
3.19	Etching and cutting circuit board.	82
3.20	Drilling the holes for fitting in the components and soldering them.	82
3.21	Design of buffer circuit for fast electric field. (a): Schematic layout designed by using ARES software. (b): Example of fabricated circuit (PCB) board. (c): Example of buffer circuit.	83
3.22	Calibrating the buffer circuit by using LeCroy Wavesurfer 3054 oscilloscope.	84
3.23	Example of calibrating results of buffer circuit. Note that the output signal (pink colour) is overlapping with the input signal (yellow colour).	85
3.24	Bandpass filter operating frequency (50 – 70 MHz).	86
3.25	Bandpass filter operating frequency (800 – 1050 MHz).	86
3.26	Bandpass filter operating frequency (50 – 70 MHz).	86
3.27	Digital PicoScope series. (a): PicoScope 4000. (b): PicoScope 5000. (c): PicoScope 6000.	87
3.28	Visual diagram of ST1.	89
3.29	Visual diagram of ST2.	90
3.30	Electric field mill Boltek EFM-100.	91
3.31	CAPPI radar format at 2 km altitude for Peninsular Malaysia for analysed storm on 12 th November 2019 at 16:20:08 (blue circle is the locations of ST1 and ST2).	92
3.32	Direction of magnetic field at the point of lightning strike and 4 quadrants (Adapted from Cooray, 2015).	94
3.33	Lightning stroke map at 50 km radius from ST1 on 12 November 2019.	96
3.34	Lightning stroke map at 50 km radius from ST1 on 24 November 2019.	97
3.35	Basic interferometer geometry (Rhodes et al., 1994; Stock e tal., 2014).	98
3.36	Effect of signal-to-noise ratio (SNR) and azimuth and elevation angle on the angular uncertainty of the broadband interferometer.	103

3.37	(a) Temporal characteristics of a stepped leader pulse (SLP) such as rise time (RT), zero-crossing time (ZCT), and total pulse duration (TPD). (b) An example of a quiet period (QP). (c) Temporal characteristics of a microwave radiation pulse such as total pulse duration (TPD), onset time, end time, and peak amplitude. (d) Temporal characteristics of a VHF radiation pulse such as TPD, onset time, end time, and peak amplitude.	105
3.38	Visual diagram of the 4G LTE performance measurement setup.	106
4.1	Location of the first return strokes on 12 and 24 November 2019 from ST1.	114
4.2	Normalized fast electric field change at 100 km (blue, FA), slow electric field change (red, SA), microwave (magenta), and very high frequency (green, VHF) detected at 3:37:45 PM on 12 November 2019.	115
4.3	Statistics of temporal characteristics of SLPs and QPs.	117
4.4	Statistics of temporal characteristics of TPD and amplitude of microwave (M) and very high frequency (VHF) radiation pulses associated with SLPs. The average values for N samples are shown on top of each box plot.	118
4.5	(a) An example of Category 1 (b) An example of Category 2 (c) An example of Category 3.	120
4.6	Total duration (TD) of QP according to categories.	121
4.7	Temporal characteristics of microwave (M) and VHF radiation pulses for Category 1 and Category 2 (C1 and C2).	122
4.8	Statistics of temporal characteristics of onset time difference; (a) between microwave pulses and SLPs, (b) between VHF pulses and SLPs, (c) between microwave and VHF pulses associated with SLPs, and (d) between microwave and VHF pulses associated with QPs.	124
4.9	Locations of -NBEs.	126
4.10	CAPPI radar images on 12 November 2019 from 5:40:00 AM to 7:00:00 AM. The maximum reflectivity value of 50 dBz were detected during period A, B, C, E and H.	127
4.11	(a, b, c) Example of one, two and three peak(s) of -NBE, respectively (blue) and overlaid with VHF radiation pulses (grey). (d) Statistics of temporal characteristics of fast electric field and VHF radiation pulses of -NBEs.	129
4.12	The interferometer mapping for -NBE10 on 12 November 2019 (06:49:13 AM).	133
4.13	EFM data on 9 and 10 November 2019 showing the background electric field in kV/m versus time in hour.	135
4.14	Statistics of temporal characteristics of onset time difference; (a) between microwave pulses and -NBEs, (b) between VHF pulses and -NBEs, (c) between microwave and VHF pulses associated with -NBEs.	136

4.15	(a) Locations of ST1, ST2, and nine +NBEs plotted according to data provided by LDN and MDF (details in Table 4.5). (b) The +NBE15 waveform with significant static components (blue, FA; red, SA; black, VHF; magenta, microwave) measured at 4.63 km from ST1. (c) The +NBE12 waveform with static component recorded at ST1, and (d) the same +NBE12 waveform without static component recorded at ST2.	139
4.16	Statistics of PD, ZCT and RT of 16 +NBEs detected in tropical region. Onset time difference, (a) between microwave radiation and +NBEs, (b) between VHF radiation and +NBEs and (c) between microwave and VHF radiations associated with +NBEs.	140
4.17	The interferometer mapping for +NBE12 on 24 November 2019 (7:30:45 PM).	142
4.18	(a) Locations of +NBE8 (yellow), stepped leader pulse (SLP2, green) and return stroke (RS1, magenta) with the distance from ST1 (blue) and ST2 (red). The background shows the intensity of the cloud obtained from the CAPPI radar provided by MMD. (b) Electric field (blue) and magnetic field (green) waveforms for the NBE3 that initiated IC and -CG flash.	144
4.19	The interferometer mapping for +NBE8 on 12 November 2019 (3:18:39 PM).	146
4.20	The interferometer mapping on the fast electric field waveform that was focused on the SLP2 and RS1. The time duration between the first and second VHF radiation sources to the onset time of the RS1 are 2.08 μ s and 2.68 μ s, respectively.	147
4.21	A visual diagram of the breakdown processes of a SLP associated with Categories 1, 2, 3.	151
4.22	Explanation on how to determine Case 1 and Case 2.	154
5.1	The plots of log files show the data of throughput (Kbps), jitter (ms) and packet loss (%) at the server node in orange, blue and magenta, respectively from 18:40:00 on 26 November 2021 until 9:50:00 on 27 November 2021. The red plot shows the background electric field in kV/m. The transmitted datagram and throughput (Kbps) at the client node were plotted in green and purple colours, respectively.	162
5.2	The plots of log files show the data of throughput (Kbps), jitter (ms) and packet loss (%) at the server node in orange, blue and magenta, respectively for 15-hour measurement period from 18:40:00 on 26 November 2021 until 9:50:00 on 27 November 2021. The red plot shows the background electric field in kV/m. The transmitted datagram and throughput (Kbps) at the client node were plotted in green and purple colours, respectively.	165

- 5.3 An example of -CG detected on 29 October 2021 at 17:50:39, 13 seconds prior to the connection dropping to zero at the client node during Storm 1. Blue waveform shows the fast electric field (V/m) record of the -CG flash that starts with preliminary breakdown pulse (PBP), stepped leader (SL) process and return stroke (RS), while the magenta shows the microwave radiation (2.3 GHz) associated with the -CG flash in arbitrary unit (A.U). 166
- 5.4 The stacked column bar graphs show the flash rate on 9 November 2021 from 15:00:00 to 20:30:00 with data sampled every 10 minutes. The throughput, jitter and packet loss at the server node were plotted in orange, blue and magenta, respectively. The red plot shows the background electric field in kV/m. The transmitted datagram and throughput at the client node were plotted in green and purple colours, respectively. 168
- 5.5 The stacked column bar graphs show the flash rate on 19 November 2021 from 16:20:00 to 23:50:00 with data sampled every 10 minutes. The throughput, jitter and packet loss at the server node were plotted in orange, blue and magenta, respectively. The red plot shows the background electric field in kV/m. The transmitted datagram and throughput at the client node were plotted in green and purple colours, respectively. 169
- 5.6 The doughnut graph displays the percentages of different types of lightning flashes (-CG, +CG, -NBE, +NBE, IC) for Storms 1, 2, 3, and 4, each represented with a ring in the colors green, purple, red, and orange, respectively obtained from the flash rate using wideband system. 172
- 5.7 The relationship formulation of correlation analysis between fair- weathers (red dots) and storms and (a) minimum throughput at client node ($T_{min}/Kbps$), (b) maximum throughput at client node ($T_{max}/Kbps$), (c) maximum packet loss ($PL_{max}/\%$) and (d) maximum jitter (J_{max}/ms), where x is the index number to divide between fair- 176
weather (1-4) and storms (5-8).
- 6.1 Electric field and x-ray radiations detected by Saba et al. (2019) accompanied with high-speed camera recording. 180

LIST OF ABBREVIATIONS

4G LTE	- The Fourth Generation Long Term Evolution
BER	- Bit error rate
BLR	- Bit loss rate
BNC	- Bayonet Neill–Concelman
BPF	- Bandpass filter
CAPPI	- Constant Altitude Plan Position Indicator
CID	- Compact intra-cloud discharge
CG	- Cloud-to-ground
CLD	- Cumulative loss datagram
CPT	- Chaotic pulse train
CST	- Computer Simulation Technology
dB/dt	- Time derivative magnetic field
dE/dt	- Time derivative electric field
EFM	- Electric field mill
ET	- End time
FA	- Fast electric field antenna
FR4	- Flame Retardant 4
FNB	- Fast negative breakdown
FPB	- Fast positive breakdown
FSK	- Frequency shift-keying
FW	- Fair-weather
GPS	- Global positioning system
IB	- Initial breakdown

IC	- Intra-cloud
IEEE	- Institute of Electrical and Electronics Engineers
Iperf3	- Internet Performance Working Group Version 3
LOS	- Loss of sight
LNA	- Low noise amplifier
MCMC	- Malaysian Communications and Multimedia Commission
MDF	- Magnetic direction finder
MFB	- Mixed fast breakdown
MMD	- Malaysia Meteorological Department
NBE	- Narrow Bipolar Event
OT	- Onset time
PBP	- Preliminary breakdown process
PC	- Personal computer
PCB	- Printed circuit board
PD	- Pulse duration
PER	- Packet error rate
PMR	- Private mobile radio
PPS	- Pulse per second
QP	- Quiet period
RT	- Rise time
RS	- Return stroke
RSSI	- Received signal strength indicator
SA	- Slow electric field antenna
SINR	- Signal-to-Interference-Noise Ratio
SLP	- Stepped leader pulse
SRS	- Subsequent return stroke
ST	- Station
TD	- Total duration
TPD	- Total pulse duration



اونیورسیتی تیکنیکل ملیسیا ملاکا
 UNIVERSITI TEKNIKAL MALAYSIA MELAKA

- UDP - User datagram protocol
- UHF - Ultra high frequency
- USB - Universal serial bus
- VHF - Very high frequency
- VNA - Vector network analyzer
- Wi-Fi - Wireless fidelity
- ZCT - Zero-crossing time
- +CG - Positive cloud-to-ground
- +NBE - Positive narrow bipolar event
- CG - Negative cloud-to-ground
- NBE - Negative narrow bipolar event



LIST OF PUBLICATIONS

Baharin, S.A.S., Ahmad, M.R., Sabri, M.H.M. and Cooray, V., 2024. Very high frequency radiation emitted by negative narrow bipolar events occurred over Malacca strait. *Journal of Atmospheric and Solar-Terrestrial Physics*, 259, p.106252. (Q3 WoS SCOPUS).

Baharin, S.A.S., Ahmad, M.R., Akbar, M.A.M.J. and Cooray, V., 2024. Electromagnetic Interference from Natural Lightning on 4G Communication Links. *IEEE Access*. (Q2 WoS SCOPUS).

Baharin, S.A.S., Ahmad, M.R., Sabri, M.H.M., Alammari, A., Al-Kahtani, A.A.N., Lu, G., Kawasaki, Z. and Cooray, V., 2023. Microwave radiation associated with positive narrow bipolar events. *Journal of Atmospheric and Solar-Terrestrial Physics*, 242, p.105998. (Q3 WoS SCOPUS).

Baharin, S.A.S., Ahmad, M.R., Al-Shaikhli, T.R.K., Sidik, M.A.B., Sabri, M.H.M., Al-Kahtani, A.A.N., Mohammad, S.A., Lu, G., Zhang, H. and Cooray, V., 2022. Microwave radiation associated with stepped leaders of negative cloud-to-ground flashes. *Atmospheric Research*, 270, p.106091. (Q1 WoS SCOPUS)

Baharin, S. A. S., Ahmad, M. R., Al-Shaikhli, T. R. K., Sabri, M. H. M., Al-Kahtani, A. A., Mohamad, S. A., Cooray, V. and Sidik, M. A. B., 2021. Microwave and Very High Frequency Radiations of The First Narrow Initial Breakdown. In *2021 35th International*

Conference on Lightning Protection (ICLP) and XVI International Symposium on Lightning Protection (SIPDA), Vol. 1, pp. 01-04. IEEE. (SCOPUS).



CHAPTER 1

INTRODUCTION

1.1 Introduction

This chapter serves as an introduction to the research work in this thesis, focusing on the lightning initiation process with microwave and very high frequency (VHF) radiation emitted by lightning. Subsequently, the objectives are formulated to address the identified problem statement in this study. Specific scopes exclusive to this study are outlined to maintain focus and relevance. The contributions of this research are delineated for clarity in reading. Finally, a detailed explanation of the overall structure and configuration of this thesis is provided to enhance understanding.

1.2 Research background

Lightning stands out as one of the captivating natural phenomena on Earth, occurring in our daily lives regardless of during daylight or the rainy season. The fleeting burst of light visible is known as a flash, often accompanied by the subsequent booming sound of thunder. Notably, depending on the observer's location, the sound of thunder may be heard either simultaneously with the lightning strike or after a perceptible delay. The interdisciplinary nature of lightning has left numerous aspects of this phenomenon unknown and ripe for exploration. Lightning is an electrical discharge that occurs in the atmosphere, emitting electromagnetic fields, x-rays, gamma rays, and optical radiation. A lightning flash is composed of several processes within typical durations ranging from 0.5 to 1 second.

The process that initiated lightning flashes is called the electrical breakdown process and begins with electron avalanches peaked at microwave radiation band on a millimeter scale. Subsequently, the fusion of multiple electron avalanches leads to the formation of streamers, believed to operate at VHF radiation on a centimeter scale. As these streamers grow, they develop into leaders on a meter scale, becoming visible as intense and bright light. A recent discovery has unveiled a new type of breakdown process known as fast breakdown. This process differs significantly from conventional breakdown, primarily in the absence of a hot conducting leader channel and the occurrence of higher propagation velocities. Notably, fast breakdown has been identified in association with the high power of a particular type of cloud flash referred to as a narrow bipolar event (NBE) (Cooray, 2015; Rison et al., 2016; Tilles et al., 2019; Huang et al., 2021).

The radiation component from lightning flashes is measured utilizing a fast electric field antenna (FA), which plays a crucial role in determining the type of lightning flashes. The sensor operates within a frequency range spanning from several hertz up to 10 MHz, with a decay time constant of 13 ms. Radio sensors, with specifications between 50 to 70 MHz and 800 to 1050 MHz, are deployed to measure VHF and microwave radiation, respectively. A VHF interferometer with a two 5 m perpendicular baseline has also been constructed to observe the direction of propagation of VHF radiation sources. This setup allows for the measurement of propagation velocities and the altitude of the recorded NBEs. Additionally, a measurement campaign has been planned and conducted to observe the effects of lightning interference on Fourth Generation Long Term Evolution (4G LTE) mobile communication links. This is particularly relevant as 4G LTE data transmission predominantly operates in the microwave band and above.